ELSEVIER

Polymer 40 (1999) 6507–6519

polymer

Anchoring characteristics and interfacial interactions in a polymer dispersed liquid crystal: a molecular dynamics study

S.S. Patnaik*, R. Pachter

Air Force Research Laboratory, Materials and Manufacturing Directorate, AFRL/MLPJ, Wright-Patterson AFB, OH 45433-7702, USA

Received 25 March 1998; received in revised form 23 November 1998; accepted 1 December 1998

Abstract

Molecular dynamics (MD) simulations were carried out to gain an understanding of the interfacial interactions and the phase separation process in a polymer dispersed liquid crystalline (PDLC) system. The most important components of the PDLC system of interest are: E7 (an eutectic mixture of cyanobiphenyl liquid crystals), a crosslinked polyacrylate, and octanoic acid (OA). The miscibility of the different components was investigated and the anchoring characteristics of 4-*n*-pentyl-4′-cyanobiphenyl (5CB) molecules on the penta-acrylate polymer surface were analyzed. The effects of introducing a surfactant on the miscibility and the anchoring strengths were also studied. Bilayers of polymer and liquid crystal (LC) of different alignments, show that an amorphous 5CB structure on the polymer surface was energetically most favorable, whereas homeotropic alignment had the next higher energy and planar alignment was the least favorable. Calculated solubility parameters indicate that prior to polymerization, the prepolymer and LC are miscible and OA is equally immiscible with both of them. Upon polymerization, the polymer is no longer miscible with the LC; phase separation occurs and OA acts as a surfactant forming a layer between the polymer and the LC. Anchoring energies calculated from the interfacial tensions indicate that the LC and polymer interface is strong. On addition of the surfactant, the anchoring energy at the interface of the LC and the surfactant becomes weaker. This decrease in anchoring strength may be one of the major factors responsible for a reduction in droplet size and also a lowering of critical field for switching, both of which are observed experimentally in volume holograms made of these PDLC materials.

Keywords: Molecular modeling; PDLC; Anchoring

1. Introduction

Polymer dispersed liquid crystals (PDLCs) are dispersions of liquid crystal (LC) droplets in a polymer matrix [1]. They have many potential device applications in displays and optical shutters due to their interesting electro–optical properties. By applying an external electric field, PDLC films can be switched between translucent and transparent states. This is possible because, under the influence of external electric fields the LC directors align preferentially within the droplet. Therefore, with a suitable choice of LC and polymer, the refractive indices of the droplet and the polymer matrix can be matched, giving rise to transparent films. Upon removal of the electric field this refractive index matching is lost and light scattering occurs.

From a more fundamental point of view, PDLCs are interesting because they exhibit a behavior, which is unique to systems that consist of mesophases in confined environments. Depending on the chemical nature of the polymer and the LC, and the preparation techniques, the interface of the LC and polymer will experience different constraints with different effects on the molecular orientation of the LCs inside the droplet. There is competition between the molecular orientation induced by the surface boundary conditions and the tendency of the LC molecules to align with each other. The interplay of these boundary conditions and the nature of surface interactions influence the width of the interface, and in the limit of a small droplet radius, these interfaces occupy a significant proportion of the total volume of the droplets. Therefore, the interfacial properties (orientation and interaction of the molecules) have a significant effect on the electro-optical properties of any PDLC-based device.

The dispersion of the LC droplets in the polymer matrix is often generated by polymerization induced phase separation (PIPS) where the prepolymer and the LC are mixed together

* Corresponding author. Tel.: + 1-937-255-6671; fax: + 1-937-255-1128.

E-mail address: patnaiss@picard.ml.wpafb.af.mil (S.S. Patnaik)

0032-3861/99/$ - see front matter
PII: S0032-3861(98)00851-9

and then polymerization is induced either thermally or photochemically. The dynamics of the phase separation process is a very complex phenomenon, which is initiated by the change in the chemical potential of the constituents as a result of the polymerization process. LC droplets are formed whose growth depends on the rate of polymerization and gelation and also on the change in miscibility of the various components. However, the stabilization of the droplets depends on the anchoring properties of the droplet/polymer interface. Therefore, an understanding of the phase separation process is important because it determines the morphology of the films (shape, size and density of the LC droplets), which along with the molecular aspects such as the director orientation and surface interactions affect their electro–optical properties.

In a newly developed PDLC system [2–7], alternating layers of LC-rich and polymer-rich layers are formed by the use of a non-uniform photopolymerization. The starting mixture contains: a crosslinking multifunctional acrylate monomer (dipentaaerythrol-hydroxy-penta-acrylate (DPHPA)), LC (E7), photoinitiator (rose bengal), chain extender (*N*-vinyl pyrrolidinone), and a coinitiator (*N*-phenyl glycine). On photopolymerization there is phase separation leading to LC-rich regions made of small spherical LC droplets with diameters ranging from ≈100 to 150 nm [6]. Addition of a very small percentage of octanoic acid (OA) (4–8% by weight) to the mixture resulted in a decrease in droplet size to ≈20 to 50 nm [7]. It also led to a significant lowering of the switching voltage, a decrease in the field-on response time, and an increase in the field-off response time.

In the present study we have used molecular dynamics (MD) simulations to explore the effect of the chemical nature of the different components on the various properties of the PDLC system [2–7]. We have focused on investigating the interfacial properties and the phase separation process, both in the presence and absence of OA. An earlier theoretical study of surface free energy and nematic anchoring was found to be successful in showing systematic trends in the phase separation process as a function of temperature and concentration [8]. However, due to the mean field approximation that was used, simplistic assumptions regarding the competing molecular interactions had to be made. MD simulations that take into account the detailed chemistry of the specific molecular structure (type of LC and polymer) can be used to carry out a detailed investigation on the molecular organization and the anchoring properties and also to study the phase separation process by analyzing the miscibility of the various components. Such simulations can be further used in conjunction with studies such as those by Lin and Taylor [8] to provide a more complete picture. MD simulations also provide a means for determining the molecular parameters such as the anchoring energies which are required in the continuum theory and often not available from experimental data.

2. Molecular models

MD simulations were carried out using complete atomistic models with the analytical form of the potential energy expression [9,10] given in Eq. (1). The potential uses fourth-degree polynomials for bond stretching (term 1) and angle bending (term 2), and a three-term fourier expansion for representing the torsions (term 3). The out-of-plane coordinates are defined by the fourth term. Cross terms up to the third order have been included (terms 5–11). Coulombic interactions (term 12) represent the electrostatic interactions and the van der Waals interactions are represented by a 6–9 function. The computational results were obtained using software programs from Molecular Simulations, Inc. [11]. MD calculations were carried out with the DISCOVER® program [11] using the PCFF force field [12]. PCFF which was developed primarily for polymers and organic materials is an extension of the consistent force field, CFF91 [9,10]. All parameters in Eq. (1) are described in detail in Ref. [12]. In the PCFF force field, hydrogen bonds are a natural consequence of the standard van der Waals and electrostatic parameters, and the addition of a special hydrogen bond function has not been found to improve the fit to experimental data.

$$
\begin{aligned}
E_{\text{pot}} = & \sum_{b} \left[K_2(b-b_0)^2 + K_3(b-b_0)^3 + K_4(b-b_0)^4\right] \\
& + \sum_{\theta} \left[H_2(\theta-\theta_0)^2 + H_3(\theta-\theta_0)^3 + H_4(\theta-\theta_0)^4\right] \\
& + \sum_{\phi} \left[V_1\left[1-\cos(\phi-\phi_1^0)\right] + V_2\right. \\
& \left.\times\left[1-\cos(2\phi-\phi_2^0)\right] + V_3\left[1-\cos(3\phi-\phi_3^0)\right]\right] \\
& + \sum_{\chi} K_\chi \chi^2 + \sum_{b}\sum_{b'} F_{bb}(b-b_0)(b'-b_0') \\
& + \sum_{\theta}\sum_{\theta'} F_{\theta\theta'}(\theta-\theta_0)(\theta'-\theta_0') + \sum_{b}\sum_{\theta} F_{b\theta}(b-b_0) \\
& \times(\theta-\theta_0) + \sum_{b}\sum_{\phi}(b-b_0)\left[V_1\cos\phi + V_2\cos 2\phi\right. \\
& \left. + V_3\cos 3\phi\right] + \sum_{b'}\sum_{\phi}(b'-b_0')\left[V_1\cos\phi + V_2\cos 2\phi\right. \\
& \left. + V_3\cos 3\phi\right] + \sum_{\theta}\sum_{\phi}(\theta-\theta_0)\left[V_1\cos\phi + V_2\cos 2\phi\right. \\
& \left. + V_3\cos 3\phi\right] + \sum_{\phi}\sum_{\theta}\sum_{\theta'} K_{\phi\theta\theta'}\cos\phi(\theta-\theta_0)(\theta'-\theta_0') \\
& + \sum_{I>j}\frac{q_i q_j}{\epsilon r_{ij}} + \sum_{I>j}\left[\frac{A_{ij}}{r_{ij}^9} - \frac{B_{ij}}{r_{ij}^6}\right]. \qquad (1)
\end{aligned}
$$

E7 is an eutectic mixture of 4 cyanobiphenyl LCs: 47% of K15 (4-*n*-pentyl-4′-cyanobiphenyl, also commonly known

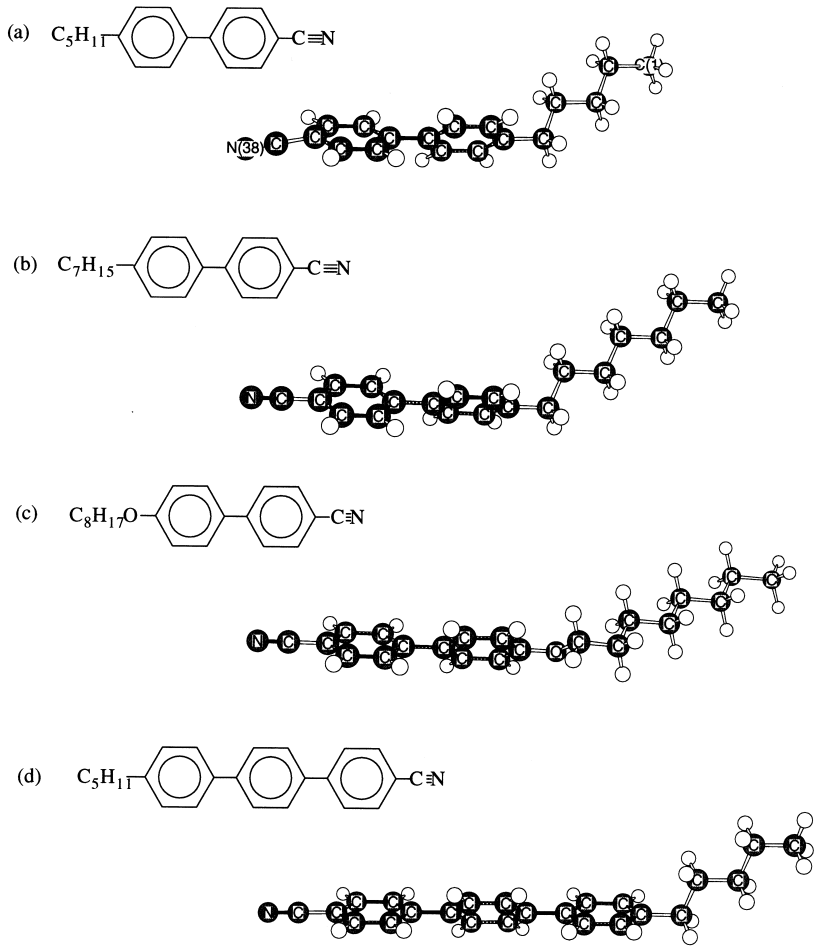

Fig. 1. Chemical structure of E7: (a) K15 (5CB, 4-*n*-pentyl-4′-cyanobiphenyl); (b) K21 (4-*n*-heptyl-4′-cyanobiphenyl); (c) M24 (4-*n*-octoxy-4′-cyanobiphenyl); (d) T15 (4-*n*-pentyl-4′-cyano-*p*-terphenyl). The filled models represent optimized geometries (not drawn to scale).

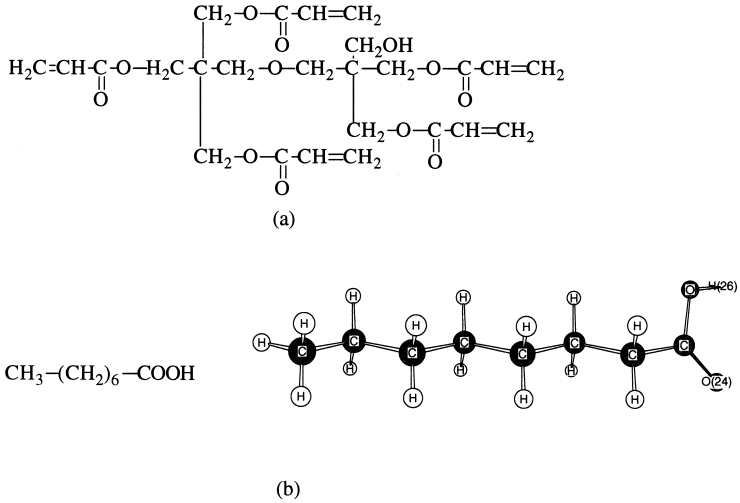

Fig. 2. (a) Chemical structure of dipentaaerythrol-hydroxy-penta-acrylate (DPHPA). (b) Octanoic acid (OA), the filled model represents the optimized geometry.

as 5CB), 25% of K21 (4-*n*-heptyl-4′-cyanobiphenyl), 18% of M24 (4-*n*-octoxy-4′-cyanobiphenyl) and 10% of T15 (4-*n*-pentyl-4′-cyano-*p*-terphenyl). The chemical structures of the different components of E7 are given in Fig. 1 and those of DPHPA and OA are shown in Fig. 2. The ratios of the molecular aspects (length/diameter) of the four LCs are in the range of 3–4. The partial charges on the nitrile group as provided by PCFF were found to be inadequate because of its rather small dipole moment. We have therefore performed a number of Hartree–Fock (HF) calculations using parallel GAMESS [13]. The 6-31G(d) basis set was utilized, which is a split valence basis set augmented by d-type polarization function on the heavy atoms. At first the geometry was optimized (optimized geometries of the LC compounds are shown in Fig. 1) and then the partial atomic charges were calculated using the Mulliken population analysis. The molecular dipole moment for 5CB(K15) was calculated to be 6.01 D. Assuming that there is a small additional contribution from the alkyl segment (dipole moment of a CH_2 group is small, of the order of 0.3 D), our calculated value is consistent with the reported experimental value of 4.34 D [14] for cyanobiphenyl in benzene solution. Other calculated values from studies using a fewer number of basis sets are 3.98 D [15] and 5.42 D [16]. The dipole moments of K21, M24 and T15 were found to be very close to that of 5CB. They were calculated to be 6.04, 6.48 and 6.26 D, respectively. It is interesting to note that the molecular dipoles are oriented primarily along the long axes of the molecules. For the purpose of comparison the dipole moment of OA was also calculated and found to be 2.07 D. Not surprisingly, due to the geometry of the carboxylic group, the net dipole moment has both a longitudinal component and a transverse component. The partial atomic charges in the nitrile group in the PCFF force field were modified to be consistent with the average calculated values for 5CB(K15), K21, M24 and T15 and were taken to be +0.2686 for carbon and −0.4546 for nitrogen (in units of electrons).

3. Methodology

3.1. Miscibility

One method of determining the miscibility of a polymer and low molecular weight molecules is by comparing their Hildebrand solubility parameters (δ), which are expressions of the square root of their respective cohesive energy densities (E_c, defined as the energy required to break all the intermolecular links in a unit volume of the material). The solubility parameter which quantifies the relative strength of the interactions between like and unlike atoms can then be related to E_c by Eq. (2) [17].

$$\delta = E_c^{1/2}. \tag{2}$$

Although a comparison of δ values can be an approximate indicator of miscibility, it does not take into account specific interactions such as hydrogen bonding as well as molecular shape and size which have significant effects on this correlation. A more rigorous approach is to calculate the free energy of mixing where a negative value would indicate miscibility:

$$\Delta H_{mix} - T\,\Delta S_{mix} < 0. \tag{3}$$

Assuming that the miscibility is determined by thermodynamics factors only and the entropy change on mixing is very small, (i.e. no significant contribution from the non-combinatorial entropy), a good prediction of miscibility may be provided by Eq. (4). The energy of mixing per unit volume (ΔE_{mix}) for a binary mixture of A and B is calculated from the differences in the cohesive energy densities of the mixed and de-mixed systems. Φ_A and Φ_B are the respective volume fractions.

$$\Delta E_{mix} = -(E_c)_{AB} + \Phi_A(E_c)_A + \Phi_B(E_c)_B. \tag{4}$$

The growth and stabilization of the phase separated LC droplets, along with being determined by the kinetic processes such as the rate of polymerization and interdiffusion of the polymer and LC molecules, also depend on the miscibility of the various components. Therefore, an understanding of the process of phase separation is very much enhanced by analyzing the miscibility of the different components as given by Eq. (4).

3.2. Anchoring characteristics

The surface anchoring (planar vs. homeotropic) and the anchoring strengths have an important role to play in the droplet sizes and the driving voltages and switching speeds of devices made of PDLC thin films. Furthermore, understanding the anchoring characteristics enables us to tailor them by adding additional components such as surfactants.

The anchoring strength of a LC at the polymer surface can be defined as the interfacial tension between the two surfaces γ_{12}, which can be further expressed as a function of individual surface tensions γ_1 and γ_2 of the two materials [17] (Eq. (5)).

$$\gamma_{12} = (\gamma_1^{1/2} - \gamma_2^{1/2})^2. \tag{5}$$

As both γ and E_c of a material depend on the same kind of intermolecular interactions, an empirical relationship (Eq. (6)) was found to be very effective in linking the two quantities [17]. Therefore, an estimate of the anchoring strength of an LC at the polymer surface can be determined by calculating the cohesive energies of the various components.

$$\gamma = 0.75E_c^{2/3}. \tag{6}$$

Table 1
Solubility parameters (δ) calculated from cohesive energies. The overall δ ($\delta = \sqrt{\delta_{ele}^2 + \delta_{van}^2}$) can be expressed in terms of contributions from electrostatics (δ_{ele}) and van der Waals (δ_{van}) which are tabulated separately

Compound	Solubility $(J\,cm^{-3})^{0.5}$	Electrostatics $(J\,cm^{-3})^{0.5}$	van der Waals $(J\,cm^{-3})^{0.5}$
DPHPA	20.9 ± 0.14	9.5 ± 0.25	18.6 ± 0.13
PMMA-6	20.9 ± 0.14	7.3 ± 0.19	19.6 ± 0.12
PMMA-65	15.9 ± 0.13	4.2 ± 0.21	15.4 ± 0.12
PMMA-100	15.5 ± 0.12	4.5 ± 0.25	14.8 ± 0.10
PMMA-200	15.4 ± 0.07	4.2 ± 0.15	14.8 ± 0.07
E7	20.0 ± 0.06	6.6 ± 0.12	18.9 ± 0.07
5CB	20.1 ± 0.05	6.6 ± 0.12	19.0 ± 0.07
5CB (LC)	20.4 ± 0.09	6.9 ± 0.09	19.2 ± 0.10
K21	19.7 ± 0.18	6.1 ± 0.14	18.7 ± 0.16
M24	19.9 ± 0.15	6.0 ± 0.17	19.0 ± 0.18
T15	19.6 ± 0.09	6.1 ± 0.15	18.7 ± 0.08
OA	22.2 ± 0.15	11.7 ± 0.3	18.8 ± 0.18

4. Computational details, results and discussion

The research was carried out in several steps. At first bulk properties were studied. An understanding of the phase separation process was achieved by analyzing the miscibility of the various components both prior to and during the polymerization. This was done by calculating the respective solubility parameters and by evaluating the energy of mixing. The molecular associations and significant atomic interactions were identified to be later compared with those at the interfaces. In the next step the interfacial properties were studied. The change in molecular alignment at the interface was investigated and the anchoring energy at the LC/polymer interface was calculated based on their cohesive energies. The effect of introducing the surfactant on the anchoring energy was also studied. In order to identify molecular phenomena that affect the anchoring characteristics, specific molecular interactions and molecular alignments at various interfaces were compared with those in the bulk material.

4.1. Bulk properties

4.1.1. Simulation details

MD simulations were carried out on samples consisting of about 1000–1500 atoms. At typical densities, such a large number of atoms were found to be sufficient to model bulk properties [12]. Three-dimensional periodic boundary conditions (pbc) along with the minimum image convention were used. In generating the amorphous structures a combination of the Theodorou and Suter method [18] and the Meirovitch scanning method [19] was used. While generating the liquid crystalline structures, mesogenic groups were defined to be the biphenyl segments in the LC molecules and then an initial structure was built where the vectors defined by the end atoms of the mesogenic segments were oriented randomly within a cone angle of 5° with respect to a specified director. Care was taken to prevent a net dipole moment of the sample box by altering the orientation of the LC molecules, both for the amorphous and the LC sample. The non-bonded interactions were truncated at 10 Å using a fifth-order spline between 9 and 10 Å to avoid discontinuities in the energies at the cutoff. A buffer width of 0.5 Å which provides the inclusion of neighboring atoms while calculating the non-bonded interactions [12] was also used. To avoid the artificial introduction of monopoles due to the cutoff, charge groups were defined and the non-bonded list was generated by including all the atoms in the charge group even if only one of them was within the cutoff range. In all cases the initial cell construction was carried out at a reduced density and then the cell was compressed to the desired density using constant pressure MD. Five starting structures were generated in each case.

To get equilibrated structures, MD simulations were carried out at 300 K under constant NVT conditions and the temperature was controlled using Anderson's method [12]. The equations of motion were integrated using the Verlet velocity integrator and a time step of 1 fs was used. Equilibration was carried out for 60 ps followed by a data collection period of 10 ps. This protocol was followed for all the five starting structures and then the properties were averaged.

4.1.2. Miscibility

4.1.2.1. Solubility parameter

Amorphous cells of E7 consisting of 19 molecules of 5CB(K15), nine molecules of K21, nine molecules of M24 and three molecules of T15 (in accordance with the molecular weight ratio of the different constituents in the eutectic mixture) in a rectangular cell with dimensions of 22.6, 22.6 and 32.2 Å corresponding to the experimental density of 1.008 $g\,cm^{-3}$ were generated. For the purpose of comparison, separate amorphous cells were also generated for all the four pure LCs: 26 molecules of 5CB were assembled in a rectangular box having the dimensions

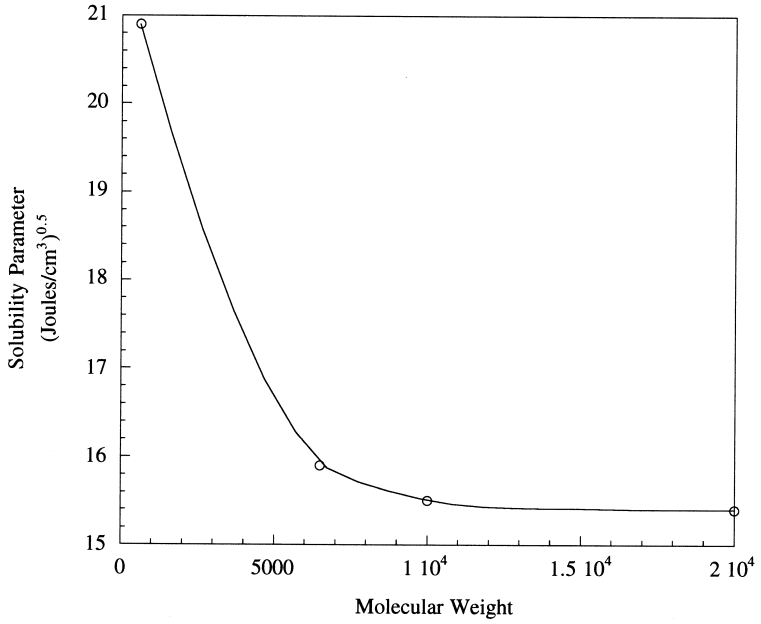

Fig. 3. Variation in the solubility parameter of PMMA with increasing molecular weight.

18.12, 18.12, and 32.52 Å; 22 molecules of K21 were assembled in a rectangular box having the dimensions 18.12, 18.12, and 30.61 Å; 20 molecules of M24 were assembled in a rectangular box having the dimensions 18.12, 18.12, and 30.84 Å; and 19 molecules of T15 were assembled in a rectangular box having the dimensions 18.12, 18.12, and 31.02 Å; all corresponding to a density of 1.008 g cm^{-3}. A different set of 5CB molecules with liquid crystalline order was also generated and their properties compared with those derived from the amorphous structure. 45 molecules of OA were assembled in a rectangular box having the dimensions 18.33, 18.33, and 35.28 Å corresponding to a density of 0.9088 g cm^{-3} [20]. 11 molecules of DPHPA were assembled in a box having the dimensions 17.6, 17.6, and 28.1 Å corresponding to a density of 1.1 g cm^{-3}.

On polymerization DPHPA crosslinks and forms a polymer with very high molecular weight. As it is difficult to generate an atomistic model of a crosslinked polymer, in order to study the miscibility of the LC with the polymer as polymerization proceeds, we have investigated the change in solubility of atactic PMMA with an increasing degree of polymerization (DP). PMMA, whose experimentally measured solubility is available in the literature, was chosen because of its close proximity with the chemical structure of DPHPA. Four different cases, PMMA-1 (DP = 6, molecular weight close to that of DPHPA), PMMA-2 (DP = 65), PMMA-3 (DP = 100), and PMMA-4 (DP = 200) were modeled.

The cohesive energy densities were calculated and then the solubility parameters evaluated (shown in Table 1) using Eq. (2). As the liquid crystalline nature of the cyanobiphenyls is uncertain for very small droplets (especially at the interface with a polymer matrix), most of the simulations were carried out starting from amorphous models. It is also interesting to note that δ of DPHPA is very close to that of PMMA-1. Fig. 3 shows the variation in δ for PMMA with the change in molecular weight. As expected after an initial steep drop, δ levels off as the molecular weight increases. The δ of high molecular weight PMMA (PMMA-4) was calculated to be 15.4 (J cm^{-3})$^{0.5}$. This is somewhat lower than the experimental value for PMMA of unspecified tacticity, which was reported to be 17.6 (J cm^{-3})$^{0.5}$ [21]. Theoretical studies [22] have reported the δ values of isotactic PMMA to be 17.3 (J cm^{-3})$^{0.5}$ and syndiotactic PMMA to be 16.3 (J cm^{-3})$^{0.5}$. In the light of this variation in the values due to the difference in tacticity, our calculated result of 15.4 (J cm^{-3})$^{0.5}$ for atactic PMMA is in reasonably good agreement with the literature values.

The close magnitude of δ values for DPHPA and E7 suggests that the two components would be miscible at the beginning of the polymerization process. During curing, as the molecular weight of the polymer increases, and its δ decreases, this mutual compatibility would decrease. This change in the δ values is expected to aid the phase separation process.

When OA is added to the mixture of DPHPA and E7, it is phase separated from the monomer and LC mixture (note the difference in δ values which indicate that OA would be equally immiscible with E7 and DPHPA). As polymerization proceeds, the relative immiscibility of OA with the polymer increases compared to that with E7, thereby favoring the formation of a coating of OA molecules around the LC droplets. As OA acts as a surfactant, even the addition of a small fraction of OA can lead to a significant change in the electro–optical properties observed experimentally [7].

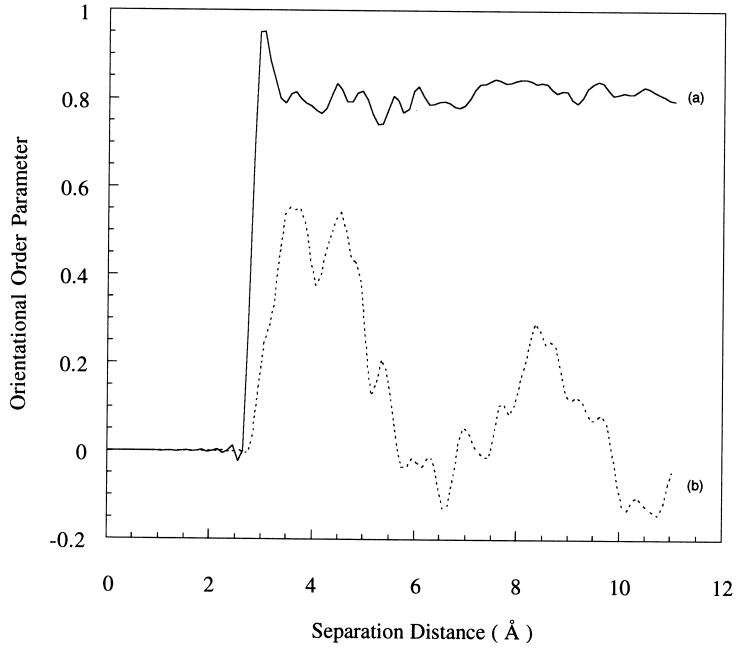

Fig. 4. Orientational order parameter P_2r: (a) 5CB with LC order; (b) 5CB with amorphous order.

4.1.2.2. Energy of mixing

In order to study the miscibility of OA with the LC and the monomer in more detail, and also for obtaining a quantitative estimate of its miscibility as a function of concentration, the energy of mixing was calculated for various cases using Eq. (4). 5CB were chosen as a representative LC and all the simulations for LCs were carried out with 5CB. The weight fractions are based on experimental weight fractions [6].

5CB (A) and OA (B): $(E_{coh}/V)_{AB}$ was calculated from an amorphous cell having dimensions 22.7, 22.7, and 20 Å. Two cases were considered which represent the two extreme range of weight fractions used in Ref. [6]. (I) $\phi_A = 0.88$ and $\phi_B = 0.12$ where $(\Delta E/V)$ was calculated to be 2.78 cal cm^{-3}. (II) $\phi_A = 0.826$ and $\phi_B = 0.174$ where $(\Delta E/V)$ was calculated to be -1.837 cal cm^{-3}.

DPHPA (A) and OA (B): $(E_{coh}/V)_{AB}$ was calculated from an amorphous cell having dimensions 22.13, 22.13 and 33.24 Å. For $\phi_A = 0.89$ and $\phi_B = 0.11$ $(\Delta E/V)$ was calculated to be -0.51 cal cm^{-3}.

PMMA-4 (A) and OA (B): $(E_{coh}/V)_{AB}$ was calculated from an amorphous cell having dimensions 25, 25 and 80 Å. For $\phi_A = 0.89$ and $\phi_B = 0.11$ $(\Delta E/V)$ was calculated to be 33 cal cm^{-3}. Such a high value of energy of mixing would indicate that under equilibrium conditions the OA would be mostly phase separated out of the polymer.

These results indicate that a comparison of the δ values for 5CB, DPHPA, and OA, does not necessarily provide a complete picture of the miscibility of the various components because the energy of mixing is also concentration dependent. At the initial stage of mixing, at a low concentration of OA ($\phi_B = 0.11/0.12$), OA seems to be slightly more miscible with DPHPA than with 5CB but, as the polymerization proceeds the polymer matrix becomes highly immiscible with OA. Similar results were also suggested by the solubility data. Our simulations provide us with a systematic qualitative understanding of the various molecular level phenomena that affect the bulk properties such as miscibility and anchoring strengths.

4.1.3. Intermolecular atomic interactions

The alignment of the LC molecules in the droplet and at the interface has a significant effect on the switching voltages. One of the major factors that affect this alignment is the specific interaction between various molecules. Prior to studying the interactions at the interface, significant interactions in the bulk material were analyzed by calculating the atomic pair distribution functions g_{ij} from the MD simulations. The atomic pair distribution function g_{ij} for a specific pair is defined so that the quantity $1/V(4\pi r^2)g_{ij}(r)\,dr$ is equal to the probability of finding atoms i and j in the distance interval r to $r + dr$ in a volume V. Therefore the number of nearest neighbors j within a distance of $|r_1 - r_2|$ for an atom i at position r can be calculated to be equal to $4\pi\rho \int r_1 r^2 r^2 g_{ij}(r)\,dr$, where ρ is the number density of i atoms in the system.

Models of both liquid crystalline 5CB and amorphous 5CB were studied because, eventually, we want to compare the atomic interactions present in the bulk material with those at the interface. The chemical nature of the polymer and the LC as well as the processing conditions are expected to influence the LC alignment at the interface. Although some studies have indicated surface alignment of both

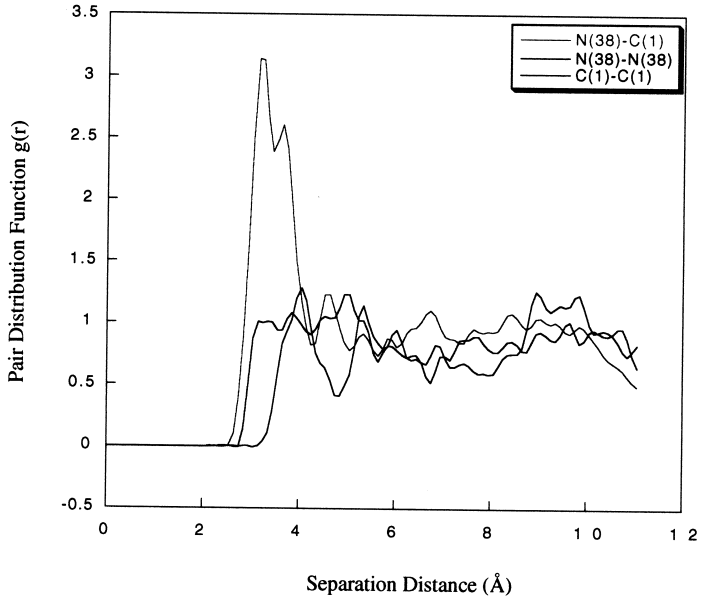

(a)

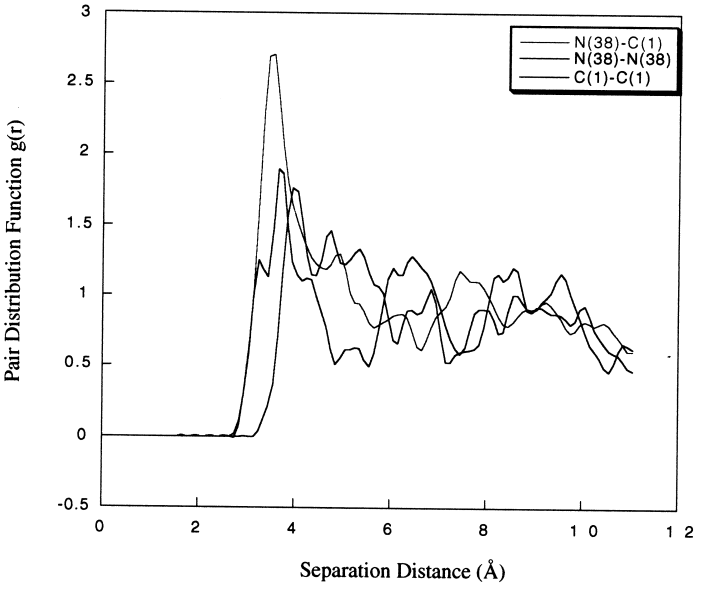

(b)

Fig. 5. Intermolecular atomic pair distribution function in: (a) 5CB (LC); (b) 5CB (amorphous).

glassy polymers [23] and cyanobiphenyls [15,24] on graphite surfaces, the liquid crystalline nature of 5CB is not very well understood at polymer surfaces, particularly one which lacks inherent surface ordering.

4.1.3.1. 5CB (liquid crystal)

Bulk 5CB is known to form a nematic LC phase between 296 and 308 K. The orientational order present in the model samples was investigated by analyzing the second-rank orientational order parameter $P_2 = \langle \frac{1}{2}(3\cos^2\theta - 1)\rangle$, where θ was chosen to be the angle between the C–N bonds of various molecules. The average was taken over the entire trajectory during the data collection stage for all the five starting configurations. The choice of the C–N bonds for calculating P_2 for 5CB (a flexible molecule) means that we are looking at the orientational order of a select fragment of the molecule. This choice is not limiting because our main purpose is to investigate the change in orientational order of 5CB in the presence of OA and the polymer surface and not to calculate its absolute P_2. Also, we are particularly interested in the orientation of the

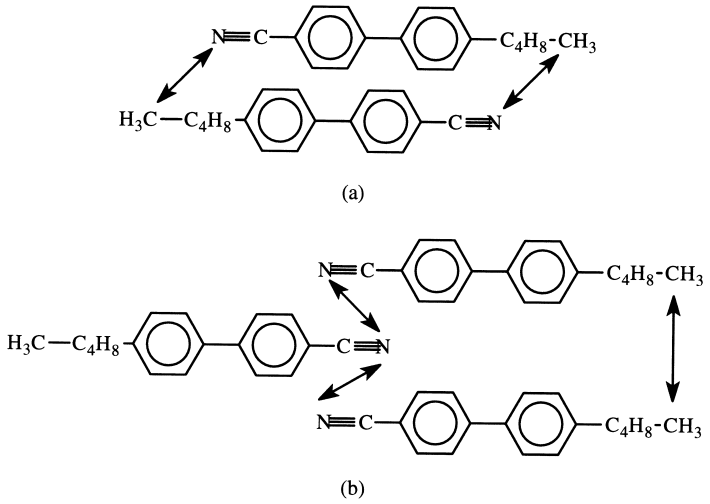

Fig. 6. Schematics representation of molecular associations found in 5CB: (a) both in amorphous and liquid crystalline; (b) only in amorphous.

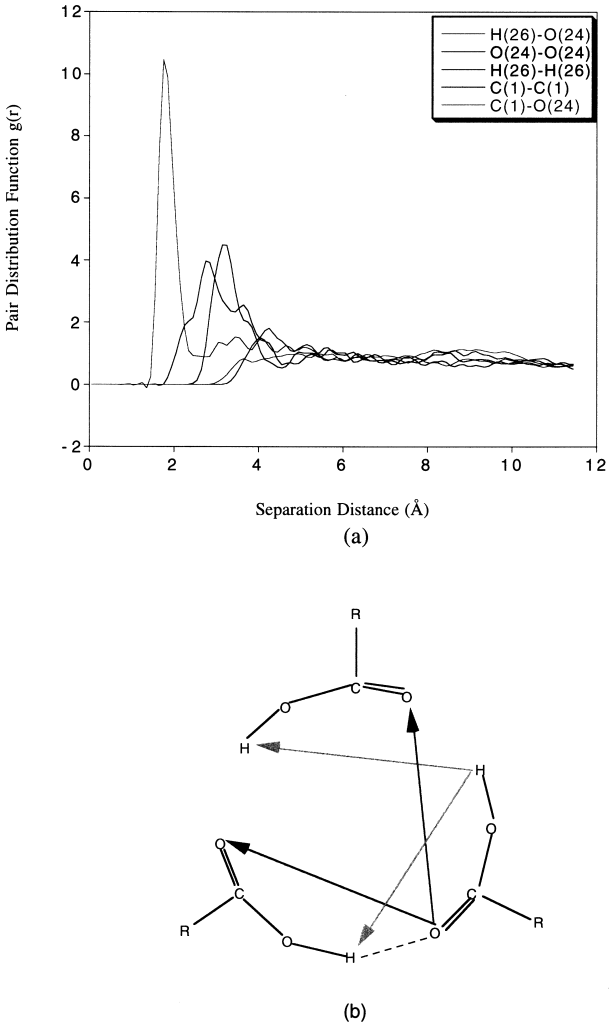

Fig. 7. (a) Intermolecular atomic pair distribution function in OA. (b) Schematic of trimerization in OA.

molecular dipole, which affects the response of the LC to an electric field. Fig. 4(a) shows that P_2r is constant (0.809 ± 0.024) over r, indicating that the system is in equilibrium. This value is larger than the value of 0.72 cited in Ref. [25], which was calculated with the long molecular axis defined for two cases, one as the *para* axis in the biphenyl segment, and another based on an inertial frame (using the molecular moment of inertia tensor), which is still higher than the experimentally measured value of 0.57 [26] using NMR, focusing on the orientation order of the *para* axis. The discrepancy between our results and those available in the literature [25] is not surprising as the earlier studies [14] show that the choice of different definitions for the molecular coordinates can have a significant effect on the calculated values of P_2r. Further, unlike our simulations with all the explicit atoms, in the work of Komolkin et al. [25], a united atom method was used.

The intermolecular atomic pair distribution functions for N(38)···C(1), N(38)···N(38), and C(1)···C(1) interactions are shown in Fig. 5(a). Only the N(38)···C(1) interactions show a strong peak ≈3.4 Å. This is consistent with a high probability of finding antiparallel associations of neighboring 5CB molecules with a tendency of the aromatic cores to form layers (Fig. 6(a)). This has also been found in the previous studies [14,25,27,28]. X-ray diffraction results report an intermolecular spacing close to 5 Å [14] which is larger than the 3.4 Å found from our study. However, we note that due to the flexible nature of the alkyl tail [14,29], the N(38)···C(1) distance does not actually represent the intermolecular distance which was measured to be the distance between the biphenyl segments [14]. In our simulations, the biphenyl segments were found to be ≈4.5 Å apart.

4.1.3.2. 5CB (amorphous)

The orientational order present in samples starting from

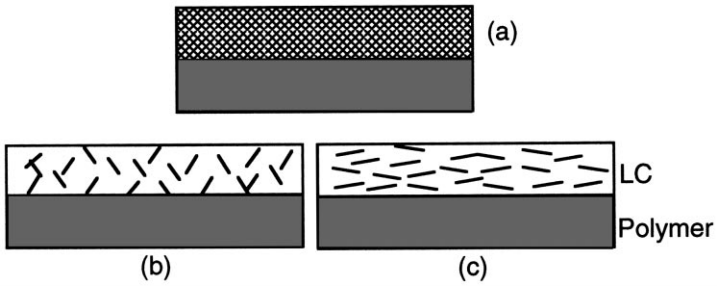

Fig. 8. Schematic of LC/polymer bilayers: (a) 5CB with amorphous 5CB on the polymer surface; (b) 5CB with homeotropic alignment on the polymer surface; (c) 5CB with planar alignment on the polymer surface.

an amorphous structure is shown in Fig. 4(b). As expected, no orientational order develops over the time of the simulation. There is a slight difference in the pair correlation functions when compared to that of the liquid crystalline state (Fig. 5(b)). Although a sharp peak is observed corresponding to the N(38)···C(1) interactions, broad peaks were also observed for N(38)···N(38), and C(1)···C(1) interactions. The number of closest nearest neighbors was calculated to be one for N···C, N···N and C···C interactions. This is consistent with an equal probability of finding antiparallel associations of neighboring nitrile groups in two different arrangements as shown in Fig. 6. The arrangement shown in Fig. 6(b) has also been observed in studies of monolayers of cyanobiphenyl molecules on a graphite surface [15]. Thus, in both the liquid crystalline and the amorphous starting structures, the nitrile groups are arranged in an antiparallel fashion indicating that their molecular dipoles play an important part in the molecular associations. The potential energy of amorphous 5CB was found to be ≈35 kcal/mol larger than that of liquid crystalline 5CB, thus supporting the fact that bulk 5CB is observed to be liquid crystalline at room temperature.

4.1.3.3. Octanoic acid

Radial distribution functions (Fig. 7(a)) show very strong intermolecular first neighbor correlations between the O(24)···H(26), H(26)···H(26) and O(24)···O(24) atoms, as indicated by peaks at 1.81, 2.8 and 3.2 Å, respectively. In this case, the hydrogen atoms refer to hydroxyl hydrogens only and the oxygen atoms to the double bonded oxygen atoms. The close proximity of the O(24),H(26) atoms from neighboring molecules, strongly support the presence of hydrogen bonding formation between the OA molecules. The number of closest nearest intermolecular neighbors calculated for the H···H interactions was found to be one, whereas those calculated for the O···O and O···H were found to be two. One possible explanation for this phenomenon could be the presence of trimers of OAs in a cyclic arrangement (schematic shown in Fig. 7(b)). This is not very surprising as the simplest carboxylic acids are known to be mainly dimerized [30]. The lack of any other peaks apart from the strong first ones in Fig. 7(a) also indicates that except for hydrogen bonding the structure remains essentially featureless, being very similar to the initial amorphous structure.

4.1.3.4. Mixture of 5CB and octanoic acid

Radial distribution functions for intermolecular interactions between 5CB and OA in a mixture of 5CB and OA do not show any significant peaks indicating that no preferred orientation is present between the two molecules.

4.2. Interfacial properties

4.2.1. Simulation details

Different cells were generated using 2d pbc which use a potential gradient method [31] (a steep potential is employed at the cell face normal to the surface region in order to confine the molecules within the box) and pbc are used in the other two directions. Two such cells, one made of molecule A and another of molecule B, were layered to form a bilayer that simulates the AB interface. The densities of the individual layers were taken to be the same as the bulk densities. Different interfaces were thus simulated and MD simulations using 3d pbc were carried out on the bilayers for 60 ps followed by a data collection period of 10 ps. Owing to the use of a steep potential (at the surface) while generating the cells, there is a region of very low density at the exact interface ($z = 0$), at $t = 0$. During the course of the simulation, this density increases and reaches an equilibrium value. This method therefore allows for creation of a rough interface. The thickness (z) of the individual layers was always taken to be greater than 20 Å because it was shown [31,32] that, there is a steep change in density and bulk properties within 10 Å of a surface. Although we are studying interfaces and not free surfaces, a conservative estimate of the layer thickness was maintained to avoid system size effects.

Unlike the model based on PMMA with a high DP that was used for calculating the solubility parameters, the polymer surface was simulated by a layer of DPHPA molecules. This was done to facilitate a faster diffusion between the DPHPA layer and the molecules of the neighboring layer (either LC or OA). The choice of DPHPA molecules as opposed to the crosslinked penta-acrylate does not necessarily imply a very simplistic model because

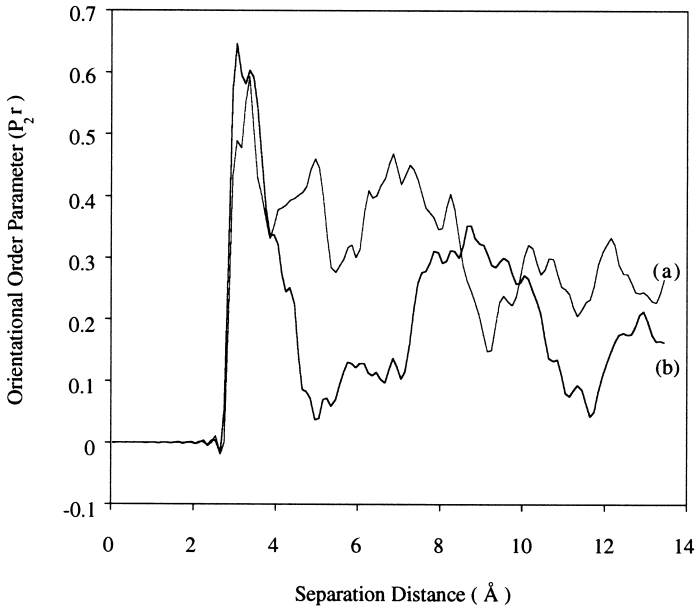

Fig. 9. Variation in orientational order parameter P_2r of 5CB in the presence of DPHPA surface: (a) homeotropic 5CB; (b) planar 5CB.

we are primarily interested in the atomic interactions between various molecules at a local level. The main interacting units in the crosslinked penta-acrylate are also present in DPHPA. A 30 Å thick amorphous layer of DPHPA was generated using the earlier mentioned potential gradient method with 2d pbc.

5CB surfaces with three different alignments were generated, namely, amorphous, homeotropic (director alignment is normal to the free surface), and planar (director alignment is primarily on the plane of the free surface) alignments. In each case a 30 Å thick layer was modeled. A 30 Å thick 2D OA surface with all amorphous structure was also generated. The various interfaces were simulated by layering two surfaces together and then the bilayers were equilibrated using MD as described in the first paragraph of this section.

4.2.2. Molecular alignment at interfaces

Schematics of the LC/polymer bilayers are shown in Fig. 8. The lowest energy was found for the amorphous LC on the polymer. It was ≈16 kcal/mol lower than that for the homeotropic alignment, which had an energy ≈44 kcal/mol lower than the planar alignment. The orientation order parameter (P_2r) was monitored for both homeotropic and planar alignments in the presence of the DPHPA surface and it was found (Fig. 9) that unlike graphite which induces ordering in cyanobiphenyls [24], the penta-acrylate surface breaks the alignment in 5CB. Note that in the absence of the penta-acrylate, P_2r remains constant as shown in Fig. 4(a). This is consistent with the low energy of the amorphous 5CB on the DPHPA surface. Similar conclusions have also been derived from experimental results using a paramagnetic resonance spin probe study on the interfacial region between E7 and PMMA [33]. These results indicate that for the small droplets of interest where there is a large interfacial area, the presence of the polymer causes a very low ordering of the LC at the interface. In bulk LC, more ordered alignment is preferred and as our results show that homeotropic alignment on the polymer is energetically more favorable than planar alignment, it is likely that for droplets which are above a critical size a radial director configuration inside the droplet could develop to reduce the strain energy while still maintaining very low ordering on the surface. Some indication of such configurations has also been observed experimentally [4].

4.2.3. Atomic interactions at interfaces

The atomic pair correlation functions based on the end atoms of 5CB, starting from both homeotropic and planar alignments on the polymer surface show a deviation from the molecular associations observed for the liquid crystalline structure towards that observed for the amorphous state. For the bilayer, as shown in Fig. 8(a) (with amorphous 5CB), the atomic pair correlation functions do not show any particular preferred molecular orientations of 5CB with respect to the penta-acrylate surface, whereas for those shown in Fig. 8(b) and (c) (liquid crystalline 5CB) there seems to be a slightly higher probability of the aliphatic tail of 5CB to be close to the polymer surface.

In the presence of the surfactant two new interfaces were created, the 5CB/OA and the OA/polymer interface. Specific molecular interactions were analyzed by monitoring the atomic pair correlation functions. For the 5CB (amorphous)/OA bilayer, the molecular associations in 5CB and OA remained unchanged as compared to those in the bulk. Further, OA was not found to induce any ordering in

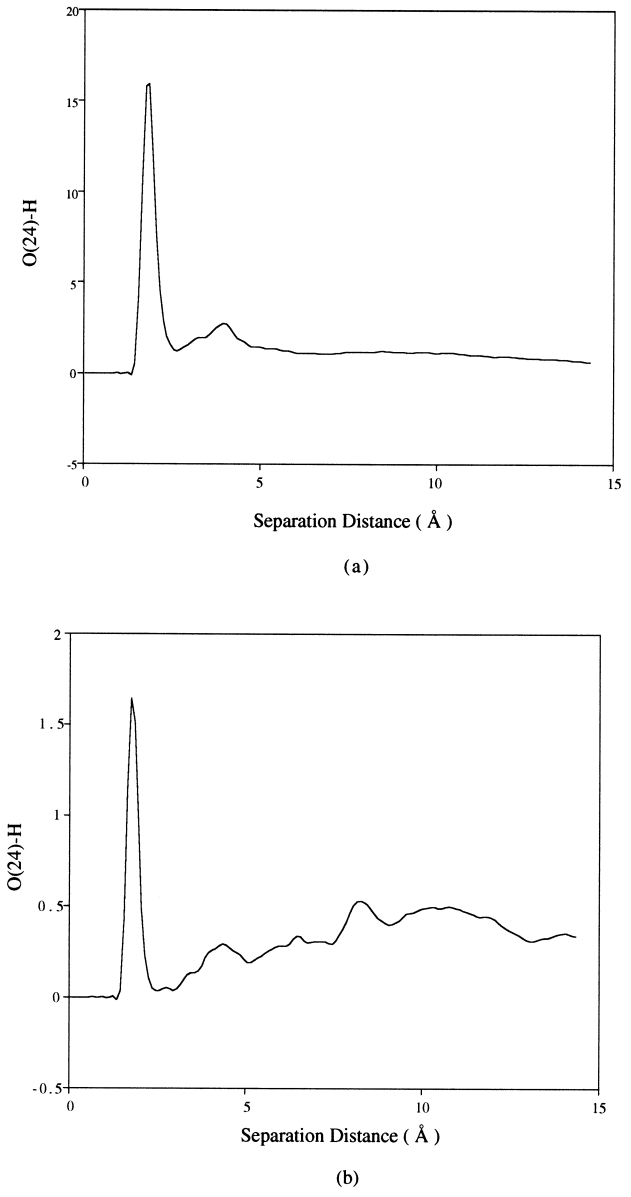

Fig. 10. Intermolecular atomic pair correlation in OA/DPHPA bilayer. The H atoms refer to the hydrogen atom in the hydroxyl group in OA: (a) hydrogen bonding within OA molecules; (b) hydrogen bonding between OA and DPHPA molecules. O(24) in the present case refers to the double bonded oxygen atoms in the acrylate group of DPHPA.

5CB. A completely different picture emerged at the OA/polymer interface. Along with forming hydrogen bonding within OA molecules, OA forms hydrogen bonding with the DPHPA surface (Fig. 10), thereby creating a strong interface with the polymer surface. The inter-molecular hydrogen bonding within OA molecules is much stronger than the hydrogen bonding of OA with the DPHPA surface, indicating that a large proportion of OA is present as aggregates. This has also been indicated by our miscibility results. As the carboxylic acid group in OA is responsible for the formation of hydrogen bonding, leading to both clustering in OA and strong interfacing with the polymer surface, there is a higher probability of the hydrocarbon tails of the OA to be oriented towards the LC surface. On application of an external electric field the weaker LC/OA interface allows for easier reorientation of the LC molecules at the interface.

4.2.4. Anchoring strength

Assuming that the bulk cohesive energy density is the same as that on the surface, the anchoring energies γ_{12} were calculated using Eqs. (5) and (6). In the absence of OA, the anchoring energy for the 5CB /DPHPA interface is reasonably strong and was calculated to be 10.74×10^{-4} J m^{-2}. Corresponding to this value of γ_{12}, a typical [6] spherical droplet of 50 nm radius, and a K (elastic constant) value of $\approx 10^{-11}$, the anchoring free energy of the droplet (which scales as the anchoring energy density times the surface area) was calculated to be approximately 35 times larger than the elastic free energy (which scales as the elastic free energy times the volume). This indicates that the anchoring coefficient is a very important factor in determining the droplet structure. On adding OA, the LC surface gets modified, and γ_{12} for the 5CB /OA interface is reduced to 3.05×10^{-4} J m^{-2}. Therefore, OA acts like a typical surfactant, which at a low concentration helps in reducing the surface tension. If the main driving force behind the change in droplet size of the LC is the surface anchoring energy, this would lead to a decrease in droplet size by half under the condition of complete phase separation of the polymer and LC. However, experimental results [6] show a more significant decrease in the droplet size, possibly indicating an incomplete phase separation. The decrease in droplet size could account for a decrease in scattering as is observed in volume holograms [6].

5. Conclusions

Atomistic simulations were able to provide us with some insight into the behavior of a PDLC system of interest. Calculated solubility parameters indicate that prior to polymerization, the prepolymer and LC are miscible and the surfactant is equally immiscible with both the monomer and the LC. Energy of mixing studies show that this miscibility is very sensitive to the concentration ratio of the different components. On polymerization the polymer is no longer miscible with the LC and the relative immiscibility of the surfactant with the polymer increases compared to that with the LC, thereby favoring the formation of a coating of OA around the LC droplets. On phase separation the surfactant forms a layer between the polymer and the LC. The molecular associations in bulk 5CB and OA were found to be consistent with those available in the literature. As OA acts as a surfactant, even the addition of a small fraction of OA can lead to a significant change in the electro–optical properties as observed experimentally [7].

Anchoring energies calculated from the interfacial tensions at the interfaces indicate that the anchoring energy

at the interface of the LC and the polymer is strong. On addition of the surfactant, the surfactant molecules form hydrogen bonding among themselves and with the polymer and the anchoring energy at the interface of the LC and the surfactant becomes weaker. This decrease in anchoring strengths might be responsible for the reduction in droplet size and a lowering of switching voltage as observed experimentally [7]. On analyzing the bilayers of polymer and the LC with different alignments, it was found that amorphous 5CB was energetically most favorable on the polymer surface, homeotropic alignment had the next higher energy and planar alignment was the least favorable. We also show that the presence of the polymer breaks the liquid crystalline alignment close to the interface. Atomic pair correlation functions do not show any preferred atomic interactions between the LC and the polymer or the LC and the surfactant. The understanding provided by our MD study, which explores the effect of the chemical nature of the various components on the anchoring characteristics as well as the phase separation process, is promising for designing PDLC systems with desirable properties.

Acknowledgements

Useful discussions with Drs L.V. Natarajan, T.J. Bunning, R.L. Sutherland and Paul Day are gratefully acknowledged.

References

[1] Drzaic PS. Liquid crystal dispersions. Singapore: World Scientific Publishing, 1995.
[2] Bunning TJ, Natarajan LV, Tondiglia V, Sutherland RL, Vezie DL, Adams WW. Polymer 1995;36:2699.
[3] Bunning TJ, Natarajan LV, Tondiglia V, Sutherland RL, Haaga R, Adams WW. SPIE Proceedings Series 1996;2651:44.
[4] Iannacchione GS, Finotello D, Natarajan LV, Sutherland RL, Tondiglia VP, Bunning TJ, Adams WW. Europhysical Letters 1996;36:425.
[5] Tondiglia VP, Natarajan LV, Sutherland RL, Bunning TJ, Adams WW. Optics Letters 1995;20:1325.
[6] Natarajan LV, Sutherland RL, Tondiglia VP, Bunning TJ, Adams WW. Journal of Nonlinear Optical Physics and Materials 1996;5:89.
[7] Tondiglia VP, Natarajan LV, Neal RM, Sutherland RL, Bunning TJ. Materials for optical limiting II, materials research society symposium proceedings, 479. Washington DC: American Chemical Society, 1997 p. 235.
[8] Lin J, Taylor PL. Journal of Physical Review E 1996;49:4258.
[9] Hwang M-J, Stockfisch TP, Hagler AT. Journal of American Chemical Society 1994;116:2515.
[10] Maple JA, Hwang M-J, Stockfisch TP, Dinur U, Waldman M, Ewig CS, Hagler AT. Journal of Computational Chemistry 1994;15:162.
[11] Molecular simulations, Inc. is a provider of molecular modeling, simulation and informatics software with headquarters in San Diego, California. Molecular dynamics calculations were done using the DISCOVER program, version 96.0 as provided in Insight II, version 4.0.0.
[12] Insight II user guide, molecular simulations, Inc., San Diego, CA, 1996.
[13] Schmidt MW, et al. Journal of Computational Chemistry 1993;14:1347.
[14] Cumper CWN, Dev SK, Landor SR. Journal of Chemical Society Perkin Transactions II 1973;46:537.
[15] Komolkin AV, Laaksonen A, Maliniak A. A Journal of Chemical Physics 1994;101:4103.
[16] Cleaver DJ, Tildesley DJ. Molecular Physics 1994;81:781.
[17] Bicerano J. Prediction of polymer properties. New York: Dekker (Marcel), 1996.
[18] Theodorou DN, Suter UW. Macromolecules 1985;18:1467.
[19] Meirovitch H. Chemical Physics 1983;79:569.
[20] Weast RC. CRC Handbook. Boca Raton: CRC Press, 1986.
[21] Jones DW, Sutow EJ, Graham BS, Milne EL, Johnston DE. Journal of Dental Research 1986;65:534.
[22] Polymer modeling and property prediction. Molecular simulations, Inc., San Diego, CA, 1996.
[23] Mansfield KF, Theodorou DN. Macromolecules 1991;24:4295.
[24] Yoneya M, Iwakabe Y. Liquid Crystals 1995;18:45.
[25] Komolkin AV, Maliniak A. Molecular Physics 1995;84:1227.
[26] Sinton S, Pines A. Chemical Physics Letters 1980;76:263.
[27] Komolkin AV, Molchanov YV, Yukutseni PP. Liquid Crystals 1989;6:39.
[28] Sandstrom D, Komolkin AV, Maliniak A. Journal of Chemical Physics 1996;104:9620.
[29] Wilson M. Journal of Molecular Liquids 1996;68:23.
[30] Jones MJ. Organic chemistry. NY, USA: Norton, 1997.
[31] Mansfield KF, Theodorou DN. Macromolecules 1990;23:4430.
[32] Misra S, Fleming PD, Mattice WL. Journal of Computer Aided Material Designs 1995;2:101.
[33] Kim YC, Lee SH, West JL, Gelerinter E. Journal of Applied Physics 1995;77:191.